Supporting Information

Démoulin et al. 10.1073/pnas.1414184111

SI Text

Fluctuations of the Filaments on the Beads. In this section, we justify that single filaments cannot be resolved on confocal microscopy images without fascin. For that, we consider the diffusional degrees of freedom of the filaments. Assuming that the polymerization reaction has reached equilibrium, the filaments are at most 9 μm long (*Materials and Methods*), which is of the same order of magnitude as the persistence length of actin (1). Contour fluctuations are thus negligible compared with the orientational fluctuations of the filaments about their anchoring point on the beads. Considering in a first approximation the bulk rotational diffusion coefficient of a rigid rod (2), one finds $D_\theta \sim 0.06\ \mathrm{s}^{-1}$. During the exposure time $t = 1$ s of the image, the root mean square angular displacement is $\sqrt{2D_\theta t} \sim 0.35$ rad, corresponding to an arc of 2.8 μm described by the tip of a filament. This simple calculation shows that it is not possible to resolve single filaments in the image.

Energetic Cost of Bundles Formation. To demonstrate that the formation of bundles is energetically favored in presence of fascin, we compare here the energetic cost of bending filaments to assemble them to the energetic gain of bundling. Ferrer et al. (3) measured a dissociation energy of two actin filaments bundled together by filamin $W = 4k_BT$ per 20 nm. We assume here the same value for fascin. To evaluate the energetic cost of bending, we consider two filaments in the situation depicted in Fig. S1 (4). One filament bends with a radius R on a length s to catch the other one, which remains straight. The total length of the filaments is $L = l_1 + l_2$. The bundling energy thus writes $U_f = -W(L - l_1)$. Geometrical considerations lead to the relation $h^2 = R^2(1 - 2\cos\theta + \cos^2\theta)$. Hence an expression of R can be derived

$$R = \frac{h^2 + l_1^2}{2h} \sim \frac{l_1^2}{2h} \quad \text{if} \quad h \ll l_1. \qquad \text{[S1]}$$

Also if $h \ll l_1$, $s = R\theta \sim l_1$. The bending energy U_b then writes

$$U_b = \int \frac{\lambda_p k_B T}{R^2} ds \sim \frac{4\lambda_p k_B T h^2}{l_1^3}. \qquad \text{[S2]}$$

The balance between U_b and U_f expresses how much the filament bends to catch the other one. Thus, at equilibrium

$$\frac{\partial(U_b + U_f)}{\partial l_1} = 0 \quad \Leftrightarrow \quad -12\frac{\lambda_p k_B T h^2}{l_1^4} + W = 0. \qquad \text{[S3]}$$

With $N_{tot} = 16{,}000$ filaments per bead, the mean distance h between two filaments on a bead is given by the expression for the random close packing Φ of disks on a sphere: $\Phi = \frac{N_{tot}\pi h^2/4}{8\pi R_{bead}^2} = 0.85$, yielding $h \sim 44$ nm. With $\lambda_p = 9$ μm (1), one obtains a numerical value of l_1

$$l_1 = \left(\frac{12\lambda_p k_B T h^2}{W}\right)^{1/4} \sim 180 \text{ nm}. \qquad \text{[S4]}$$

The hypothesis $h \ll l_1$ is verified. Filaments growing with the velocity of elongation in solution $v_o = 0.42$ nm/s reach the length l_1 after 7 min of polymerization. In all experiments, filaments grow at v_o during 10 min before the magnetic field is turned on. Thus, it is reasonable to assume that all filaments are assembled into bundles at all times in the measurements.

To create a bigger bundle, filaments further apart on the surface of the bead assemble together, having to bend more and more. Because the number of filaments in a bundle saturates to 20 (5, 6), we can assume that the derivation above is valid for a whole bundle with only a slight deviation of the different parameters.

Static Mechanical Properties of the Actin Filaments Populations. A rapid ascending then descending force ramp is applied after 20 and 35 min of polymerization (Fig. S2). The whole measurement takes 100 s to complete, which is fast enough to consider the length of the filaments as constant. For each curve, the two branches corresponding to the ascending and descending force ramps are almost superimposed, indicating that the filaments are not irreversibly damaged by the force. However, the descending branch is always slightly below the ascending one. This behavior is reproducible (Fig. S3) and may be due to slowly relaxing interactions with the surface of probe beads. We notice that at forces below 1 pN, the surface-to-surface distance is similar to the filament length, suggesting that filament growth is not affected by very low load.

In the absence of fascin, filaments pivot about their anchoring point to decrease their average angle with the facing probe particle. This way they can accommodate increasingly higher loads. As a consequence, the surface-to-surface distance almost drops to 0, indicating that the actin corona can be compressed almost 100% (7). In contrast, in the bundled configuration, filaments only undergo a 30–40% compression at equivalent loads.

The Elongation Velocity of the Filaments Depends on Force. Here we observe the growth of filaments subjected to alternating periods of low and high force to show that their elongation velocity directly depends on the force applied to them (Fig. S4).

Filaments grow at high velocity under low force (phase A). As expected, when the applied force increases, the velocity decreases (phase B). Finally in phase C of low force, the velocity is restored to a similar value as the one measured in phase A. The small difference of 0.04 nm/s is not significant compared with the noise in the force-velocity profile (Fig. 2): for $F = 5.3 \pm 0.6$ pN, $v = 0.22 \pm 0.06$ nm/s (six data points, mean ± SD). The velocity thus depends only on applied force and not on the history of the system.

The surface-to-surface distance decreases slightly at the beginning of phase B because of elastic deformation (Fig. S2). After phase B, the surface-to-surface distance is restored to a comparable value as the one at the end of phase A. Again, the small difference observed (30 nm) is not significant because it is similar to the hysteresis observed in mechanical measurement (Fig. S2). This result indicates that growth is almost stopped during the high force phase B, with the filaments kept abutting the opposing bead surface. In contrast, in the absence of fascin, previous observations (7) showed that reorganization and rotation of filaments take place under high force, allowing them to grow in phase B at a force-insensitive velocity, so that they resume growth in phase C at the position that is extrapolated from the data points in phase A (arrow in Fig. S4).

Density of Filaments on the Beads. We show here that the number of filaments on the beads is not modified by the presence of fascin (e.g., bundling could impede the growth of some filaments). For that, we let fluorescent actin grow on the beads without a magnetic

field and compare the fluorescent intensity around beads in both the free and bundled configurations. The polymerization time (3 h) is long enough to assume the reaction has reached equilibrium. Protein concentrations are 6 μM Alexa488-labeled actin in the free configuration and 6 μM Alexa488-labeled actin and 2 μM fascin in the bundled configuration. Fluorescence intensity is measured with Image J software for four beads randomly chosen from different batches in each configuration. Fluorescence intensity (arbitrary units) is found to be 11,500 ± 3,300 in the free configuration and 11,600 ± 4,600 in the bundled configuration (mean ± SD). These results highlight a relatively large difference in the density of filaments from bead to bead but reveal no statistical difference between the two configurations.

Numerical Simulations. Here we discuss in more details the hypotheses and results of the numerical simulations from which we concluded that the extension of the filaments in our system proceeds by a Brownian ratchet mechanism at the single filament level. As stated in the description of the principle of the simulations (*Materials and Methods*), the system is rotation-invariant around the axis of the pair of beads and the relevant parameter is the angle θ_i between a filament i and that axis (Fig. S8*E*).

The bigger the θ_i, the smaller the work filament i has to produce to extend of a monomer length δ. Thus, the average $k_{\text{on}}(i)$ increases with θ_i, causing the filaments to elongate with different velocities and the actin corona to adopt the shape of the neighbor bead (Fig. S8 *A*–*D*).

Our numerical simulations neglect the effect of ATP hydrolysis. Indeed, contrary to the barbed end, the elongation velocity of actin filaments from the pointed end varies linearly in a wide range of monomer concentrations from below to above the critical concentration (8), which means that (*i*) either the dissociation speeds of ATP-actin and ADP-actin are equal at the pointed end or (*ii*) ATP-actin caps are never observed at growing pointed ends, at least in the region of monomer concentrations close to the critical concentration (in which we are working) where the elongation velocity is small. This would imply that hydrolysis systematically occurs quickly after the slow association of ATP-actin monomers.

Another important hypothesis in our simulations is that lateral attractive interactions between monomers due to bundling are neglected. Taking them into account could alter the distribution of filament tip distances to the load and thus the efficiency of force generation. Krawczyk and Kierfield (9) showed that, although bundling does alter the thermodynamic constants of filament polymerization, it has little influence on the simulated force-velocity profile. We thus expect the behavior of bundled filaments and stiff unbundled filaments to be hard to discriminate, and for this reason, we chose to neglect lateral attractive interactions in our model.

During the simulations, after allowing the filaments to grow in the same conditions as in the dynamic experiments, a linear fit to the surface-to-surface distance vs. time data is performed to construct the force-velocity profile. All parameters in the simulations are determined by kinetics measurements (*Materials and Methods*) except N, which is set to 130 after a least-square minimization test (Fig. S7). With all parameters fixed, we finally submit our model to a sequence of forces corresponding to the experimental conditions (Fig. S5). Due to the incompressibility hypothesis, the simulation does not predict the compression at high force. Apart from that, it reproduces every feature of the experimental curve. In particular, the separation velocity is insensitive to the history of force and the surface-to-surface distance remains almost constant during the period of high force. We conclude that the mechanism of force generation in our system is compatible with the Brownian ratchet.

Cooperation of Ratcheting Filaments Against the Load. To get more insight into the physics underlying the existence of a maximum in the power curve in Fig. 3, we calculate the average work $\langle w^+ \rangle$ that is done each time a monomer is added to a polymerizing tip situated at a distance less than δ from the load. Knowing that p_{n} is constant on the distance $[0;\delta]$ from the load (*Materials and Methods*), one obtains

$$\langle w^+ \rangle = \frac{\sum_{i=1}^{N} p_{\text{i}} F \frac{i\delta}{N} e^{-\frac{iF\delta}{Nk_{\text{B}}T}}}{\sum_{i=1}^{N} p_{\text{i}} e^{-\frac{iF\delta}{Nk_{\text{B}}T}}} = \frac{F\delta}{N} \frac{Ne^{-\frac{N+1}{N}\frac{F\delta}{k_{\text{B}}T}} + 1 - (N+1)e^{-\frac{F\delta}{k_{\text{B}}T}}}{\left(1 - e^{-\frac{F\delta}{Nk_{\text{B}}T}}\right)\left(1 - e^{-\frac{F\delta}{k_{\text{B}}T}}\right)}. \quad \textbf{[S5]}$$

For $N \gg 1$ and $F \gg k_{\text{B}}T/\delta$, the expression simplifies into $\langle w^+ \rangle \sim k_{\text{B}}T$.

The average effective distance on which the load is pushed at each monomer addition is thus $\langle x^+ \rangle \sim k_{\text{B}}T/F$. This result means that the fraction of filaments N_{eff} that can effectively push the load are situated at a distance $\delta - k_{\text{B}}T/F$ from it

$$N_{\text{eff}} = \sum_{i=1}^{\frac{k_{\text{B}}T}{F\delta}} p_{\text{i}} = \frac{v_o}{\delta k_{\text{on}} C \left(N \frac{k_{\text{B}}T}{F\delta} + \frac{F\delta}{k_{\text{B}}T} \right)} N = \frac{P}{k_{\text{on}} C}. \quad \textbf{[S6]}$$

We can thus give the following interpretation for the shape of the power curve. At forces below $F_{P_{\max}}$, the energetic cost of moving the load by big steps is rather low, so that a few filaments push the load, whereas the rest are lagging behind (Fig. S6 *A* and *B*). The power transduction is close to its maximum given by the slope at the origin $P_o = \frac{Fv_o}{k_{\text{B}}T}$, showing that this regime is limited by polymerization speed. In contrast, the regime of forces higher than $F_{P_{\max}}$ is limited by thermal fluctuations of the load. A majority of filament tips accumulate close to the wall (10, 11) (Fig. S6*C*). In the perfect work sharing scenario, any monomer addition to a filament tip produces work and moves the load of a distance δ/N (12) (Fig. S6*D*). The power transduced in this case is $P_{\text{id}} = \frac{F\delta}{k_{\text{B}}T}\left(k_{\text{on}} C e^{-\frac{F\delta}{Nk_{\text{B}}T}} - k_{\text{off}}\right)$. In our experimental system, some monomer additions result in a big step forward of the load and a large amount of work transduced, whereas others result in no movement of the load (Fig. S6*E*). As demonstrated by Schaus and Borisy, the efficiency of such a system is significantly lower (12).

1. Isambert H, et al. (1995) Flexibility of actin filaments derived from thermal fluctuations. Effect of bound nucleotide, phalloidin, and muscle regulatory proteins. *J Biol Chem* 270(19):11437–11444.
2. Brenner H (1974) Rheology of a dilute suspension of axisymmetric brownian particles. *Int J Multiph Flow* 1(2):195–341.
3. Ferrer JM, et al. (2008) Measuring molecular rupture forces between single actin filaments and actin-binding proteins. *Proc Natl Acad Sci USA* 105(27):9221–9226.
4. Kuhne T, Lipowsky R, Kierfeld J (2009) Zipping mechanism for force generation by growing filament bundles. *Europhysics Letters* 86(6):68002.
5. Ishikawa R, Sakamoto T, Ando T, Higashi-Fujime S, Kohama K (2003) Polarized actin bundles formed by human fascin-1: Their sliding and disassembly on myosin II and myosin V in vitro. *J Neurochem* 87(3):676–685.
6. Claessens MMAE, Semmrich C, Ramos L, Bausch AR (2008) Helical twist controls the thickness of F-actin bundles. *Proc Natl Acad Sci USA* 105(26):8819–8822.
7. Brangbour C, et al. (2011) Force-velocity measurements of a few growing actin filaments. *PLoS Biol* 9(4):e1000613.
8. Carlier MF, Criquet P, Pantaloni D, Korn ED (1986) Interaction of cytochalasin D with actin filaments in the presence of ADP and ATP. *J Biol Chem* 261(5):2041–2050.
9. Krawczyk J, Kierfeld J (2011) Stall force of polymerizing microtubules and filament bundles. *Europhysics Letters* 93(2):28006.
10. van Doorn GS, Tanase C, Mulder BM, Dogterom M (2000) On the stall force for growing microtubules. *Eur Biophys J* 29(1):2–6.
11. Tsekouras K, Lacoste D, Mallick K, Joanny JF (2011) Condensation of actin filaments pushing against a barrier. *New J Phys* 13(10):103032.
12. Schaus TE, Borisy GG (2008) Performance of a population of independent filaments in lamellipodial protrusion. *Biophys J* 95(3):1393–1411.

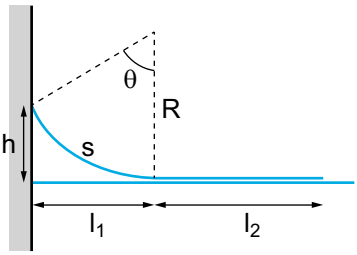

Fig. S1. Simplified geometry of a bundle of actin filaments considered for energy calculations.

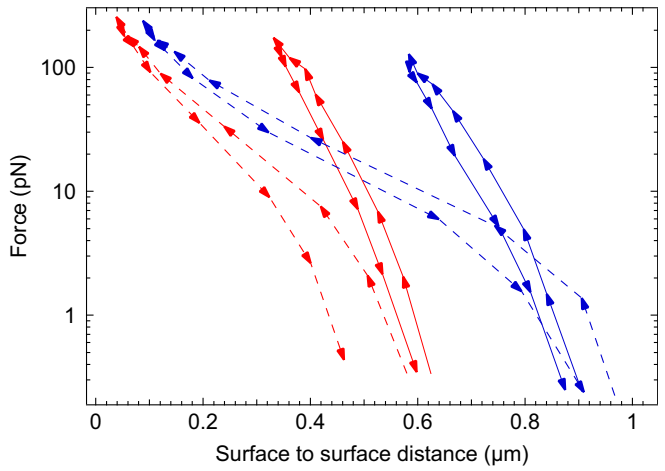

Fig. S2. Static mechanical properties of the actin filaments populations. Measurements are performed on the same chain of particles after 20 (red) and 35 min (blue) of polymerization in the free configuration (broken lines, 2 μM actin) and in the bundled configuration (plain lines, 2 μM actin and 2 μM fascin). Arrowheads indicate the ascending and descending ramps. Length of the filaments calculated from bulk kinetics measurements: 480 nm (red) and 840 nm (blue).

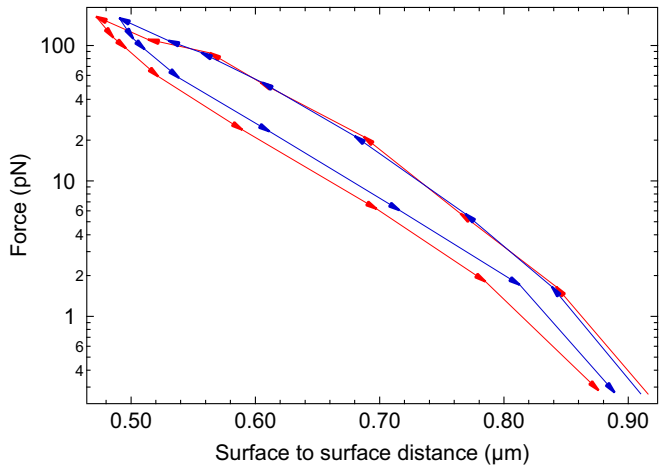

Fig. S3. Successive ascending then descending ramps of force applied to the same chain of beads in the bundled configuration (2 μM actin and 1 μM fascin). The first ramp (red line) is applied after 37 min of polymerization, corresponding to a filaments length of 890 nm. After 30 s of rest, a new ramp is applied (blue line). Arrowheads indicate ascending and descending ramps.

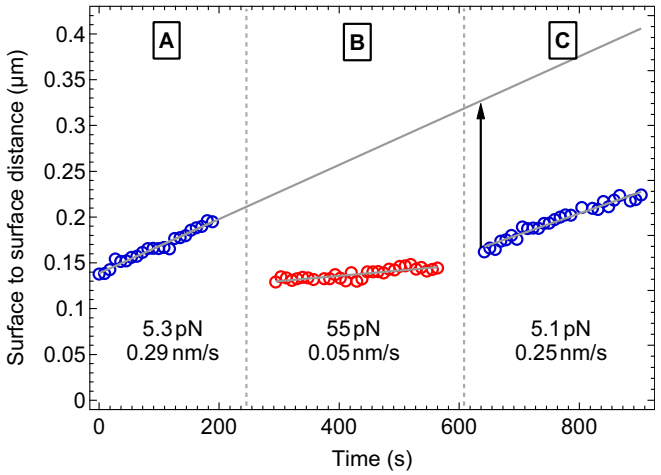

Fig. S4. Evolution of the surface-to-surface distance during the application of alternating phases of low and high forces to a chain of beads with 2 μM actin and 2 μM fascin. For each phase in the sequence, the value of the force is given, as well as the separation velocity derived from a linear fit to the data (plain gray lines). Colors distinguish the phases of low force (blue) and high force (red).

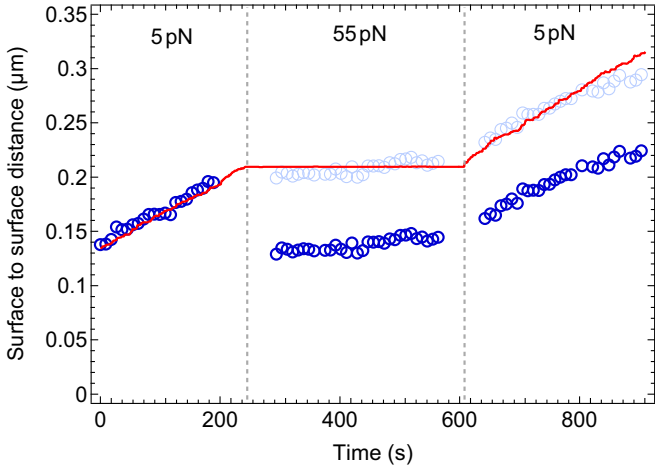

Fig. S5. Numerical simulation of the surface-to-surface distance evolution during a force sequence (red line). Experimental data for the bundled configuration are added to the figure (blue circles). For comparison with an incompressible situation, experimental data for the last two periods have been shifted by 70 nm (light blue circles).

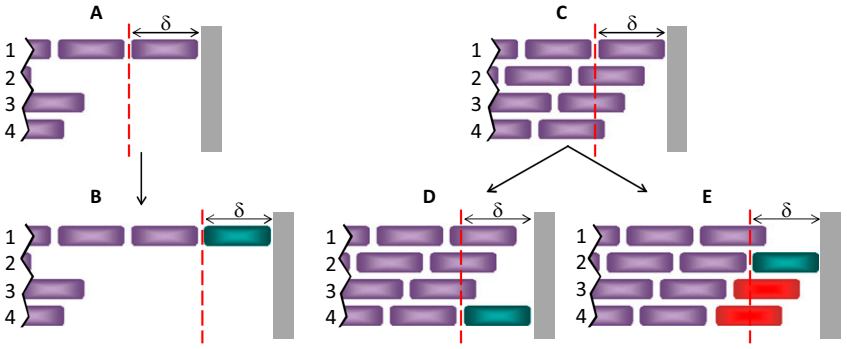

Fig. S6. Different scenarios for force production by staggered filaments. Only the filaments whose tip is at a distance less than δ from the wall can produce work. (*A* and *B*) For $F < F_{P_{max}}$, essentially one filament supports the load, whereas the rest are lagging behind, resulting in the load moving by big steps. (*C*) For $F > F_{P_{max}}$, filaments accumulate near the wall. (*D*) In an ideal ratchet, monomer attachment always occurs from the filament whose polymerization causes the minimal advance of the wall, so that each monomer addition produces work. (*E*) In a real system, sometimes a filament close to the wall can produce a big amount of work (e.g., filament 2), allowing subsequent monomer additions to occur without producing work (e.g., filaments 3 and 4) and decreasing the overall efficiency of the system.

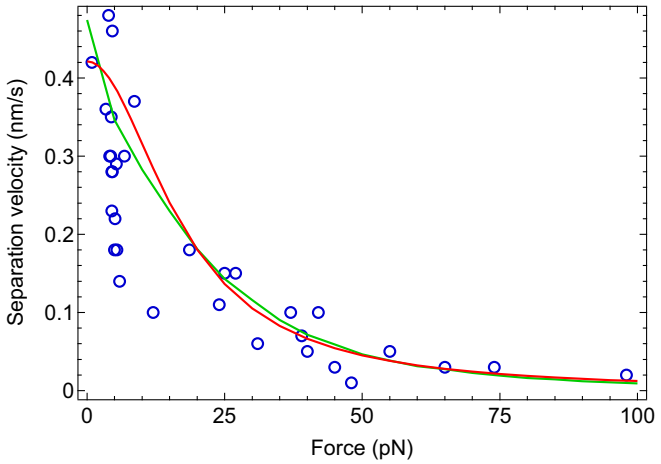

Fig. S7. Comparison of the experimental force-velocity profile (blue circles) with the simulated one (green line) and the one calculated with the expression $v = v_o / \left[1 + \frac{1}{N}\left(\frac{F\delta}{k_B T}\right)^2\right]$ derived from our analytical model (red line). In both the numerical and the analytical model, the number of filaments able to push the neighbor bead is $N = 130$.

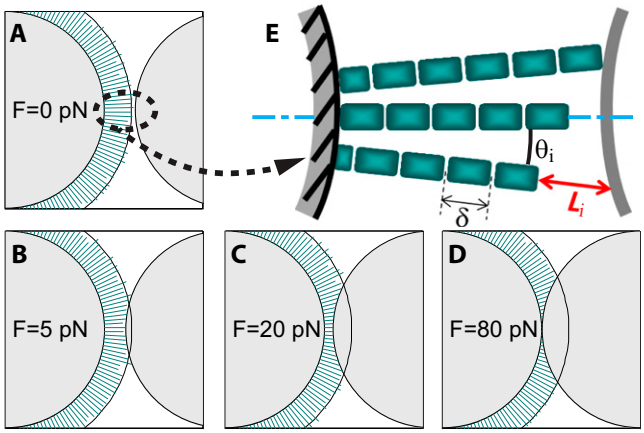

Fig. S8. (*A–D*) Cross-sectional views in the equatorial plane of the pair of particles considered in the 3D numerical simulations after filaments have polymerized 1,000 s under constant force. Filaments (green lines) are drawn to scale. The black circle represents the average length L filaments would reach if they were growing in solution: $L = v_o t = 420$ nm. (*E*) Diagram depicting how the elongation of the filaments is computed (see *SI Text*).